EBioMedicine xxx (xxxx) xxx

Contents lists available at ScienceDirect

EBioMedicine

journal homepage: www.elsevier.com/locate/ebiom

EBioMedicine
Published by THE LANCET

Research paper

SPARC dependent collagen deposition and gemcitabine delivery in a genetically engineered mouse model of pancreas cancer

Iswarya Ramu[a], Sören M. Buchholz[a], Melanie S. Patzak[a], Robert G. Goetze[a], Shiv K. Singh[a], Frances M. Richards[b], Duncan I. Jodrell[b], Bence Sipos[c], Philipp Ströbel[d], Volker Ellenrieder[a], Elisabeth Hessmann[a], Albrecht Neesse[a,*]

[a] Department of Gastroenterology and Gastrointestinal Oncology, University Medical Centre Göttingen, Germany
[b] Cancer Research UK Cambridge Institute, Li Ka Shing Centre, The University of Cambridge, United Kingdom
[c] Institute of Pathology and Neuropathology, University Clinic Tübingen, Germany
[d] Institute of Pathology, University Medical Centre Göttingen, Germany

ARTICLE INFO

Article history:
Received 9 July 2019
Revised 7 September 2019
Accepted 13 September 2019
Available online xxxx

Keywords:
SPARC
Pancreatic cancer
Drug delivery
Collagen
Chemoresistance

ABSTRACT

Background: Pancreatic ductal adenocarcinoma (PDAC) is characterised by extensive matrix deposition that has been implicated in impaired drug delivery and therapeutic resistance. Secreted protein acidic and rich in cysteine (SPARC) is a matricellular protein that regulates collagen deposition and is highly upregulated in the activated stroma subtype with poor prognosis in PDAC patients.
Methods: $Kras^{G12D}$;p48-Cre;*SPARC* $^{-/-}$ (KC-*SPARC* $^{-/-}$) and $Kras^{G12D}$;p48-Cre;*SPARC* ^{WT} (KC-*SPARC* ^{WT}) were generated and analysed at different stages of carcinogenesis by histological grading, immunohistochemistry for epithelial and stromal markers, survival and preclinical analysis. Pharmacokinetic and pharmacodynamic studies were conducted by liquid chromatography-tandem mass spectrometry (LC-MS/MS) and immunohistochemistry following gemcitabine treatment (100 mg/kg) in vivo.
Findings: Global genetic ablation of SPARC in a $Kras^{G12D}$ driven mouse model resulted in significantly reduced overall and mature collagen deposition around early and advanced pancreatic intraepithelial neoplasia (PanIN) lesions and in invasive PDAC ($p < .001$). However, detailed pathological scoring and molecular analysis showed no effects on PanIN to PDAC progression, vessel density (CD31), tumour incidence, grading or metastatic frequency. Despite comparable tumour kinetics, ablation of SPARC resulted in a significantly shortened survival in KC-$SPARC^{-/-}$ mice (280 days versus 485 days, $p < .03$, log-rank-test). Using LC-MS/MS, we show that SPARC dependent collagen deposition does not affect intratumoural gemcitabine accumulation or immediate therapeutic response in tumour bearing KC-$SPARC^{WT}$ and KC-$SPARC^{-/-}$mice.
Interpretation: Global SPARC ablation reduces the collagen-rich microenvironment in murine PDAC. Moreover, global SPARC depletion did not affect tumour growth kinetics, grading or metastatic frequency. Notably, the dense-collagen matrix did not restrict access of gemcitabine to the tumour. These findings may have direct translational implications in clinical trial design.

* Corresponding author at: Department of Gastroenterology and Gastrointestinal Oncology, University Medical Centre Göttingen, Georg-August-University, Robert-Kochstr. 40, 37075 Göttingen, Germany.
E-mail address: albrecht.neesse@med.uni-goettingen.de (A. Neesse).

https://doi.org/10.1016/j.ebiom.2019.09.024

Research in context

Evidence before this study

Pancreatic ductal adenocarcinoma (PDAC) features pronounced desmoplasia with abundant extracellular matrix (ECM) components such as collagen and hyaluronic acid that promote tumourigenesis and impede drug delivery and response. Secreted protein acidic and rich in cysteine (SPARC) is a matricellular protein that is expressed in bone, testis and connective tissues. SPARC has been functionally implicated in wound healing and collagen deposition. Interestingly, SPARC is highly expressed by peritumoural fibroblasts in PDAC. Recent high-throughput sequencing technologies have identified SPARC as a marker for the activated stroma subtype in human PDAC that correlates with poor prognosis. However, SPARC has not been investigated in genetically engineered mouse models at different precursor stages of PDAC to determine its contribution to progression and therapeutic resistance.

Added value of this study

The present study provides evidence that global SPARC ablation results in significantly reduced collagen deposition around PanIN lesions and tumours in the $Kras^{G12D}$ mouse model. Notably, SPARC dependent collagen deposition did not affect pancreatic intraepithelial neoplasia (PanIN) to PDAC progression, vascularity, proliferation, apoptosis rate, or metastatic frequency. Despite a lower tumour frequency in KC-$SPARC^{-/-}$ mice, median survival was significantly shortened compared to KC-$SPARC^{WT}$. This phenotype was likely caused by more severe clinical symptoms such as diarrhoea, jaundice and ascites upon tumour induction in KC-$SPARC^{-/-}$. Despite the prevailing hypothesis that the ECM matrix impedes drug delivery and efficacy in PDAC, liquid chromatography-tandem mass spectrometry (LC-MS/MS) and immunohistochemistry revealed comparable pharmacokinetic and pharmacodynamics characteristics for gemcitabine in KC-$SPARC^{WT}$and KC-$SPARC^{-/-}$ mice.

Implications of all the available evidence

We have investigated the role of global SPARC depletion during different stages of pancreatic tumourigenesis. Our findings show that global SPARC depletion results in comparable PanIN and tumour growth kinetics despite a more severe clinical phenotype in KC-$SPARC^{-/-}$ mice. Furthermore, our data contradict the prevailing hypothesis that the dense-collagen matrix restricts access of gemcitabine to the tumour. Thus, our findings may have direct translational implications in clinical trial design.

1. Introduction

Histologically, PDAC is characterised by abundant stroma that harbours inflammatory cells (e.g. myeloid cells), cancer-associated fibroblast (CAFs), and large amounts of extracellular matrix (ECM) components, in particular collagen and hyaluronic acid [1,2]. The extensive tumour stroma was shown to contribute towards tumour progression, therapeutic resistance and poor prognosis in PDAC [3,4]. However, it is still unclear which components of the tumour stroma contribute to disease progression, and whether this is dependent on deposition of certain ECM components during pancreatic intraepithelial neoplasia (PanIN)-PDAC progression. To this end, several preclinical experiments suggest that pharmacological depletion or remodelling of acellular components such as hyaluronic acid and collagen increases delivery of and response to antineoplastic agents [5–10]. On the other hand, recent data show no correlation between intra-tumoural gemcitabine concentrations and overall survival in a preclinical study using genetically engineered mice thus casting doubt on the biophysical drug barrier hypothesis [11]. Furthermore, the failure of numerous clinical trials using anti-stromal agents (e.g. sonic hedgehog inhibitors, matrix metalloproteinase, MMP inhibitors) has further dampened the initial euphoria of the stromal depletion strategy and fuelled scepticism whether the stromal barrier hypothesis is correct [12].

SPARC is an important matricellular protein that is overexpressed in peritumoural fibroblasts and has been associated with collagen deposition and the activated stroma subtype in PDAC [13,14]. High expression of SPARC in peritumoural fibroblasts is associated with a poor prognosis in PDAC patients [15]. Moreover, SPARC was proposed as a negative predictive factor for the treatment with gemcitabine [16]. Whether these clinical findings are causally related to SPARC or just associated with a more desmoplastic phenotype remains unanswered. Moreover, preclinical data from different mouse models show conflicting results regarding the role of SPARC in PDAC [17–21].

To investigate the role of SPARC in PDAC progression, drug delivery and response, we employed the *LSL-*$Kras^{G12D/+}$; p48-*Cre* (KC) mouse model that develops PanIN lesions at 3–4 months of age and progresses to invasive PDAC after a latency of 12–15 months [22]. Progression to PDAC is accompanied by the development of a pronounced tumour microenvironment (TME) in which ECM components such as collagen and hyaluronic acid increasingly accumulate. To test the potential of SPARC as a biomarker for gemcitabine treatment, we used a recently established and validated liquid chromatography-mass spectrometry/mass spectrometry (LC-MS/MS) assay [23–25], the most sensitive method to quantify gemcitabine metabolites in small tissue biopsies, and assess response in pancreatic tumour tissues from KC-$SPARC^{-/-}$ and KC-$SPARC^{WT}$ mice.

2. Material and methods

2.1. Genetically engineered mouse models

$SPARC^{-/-}$ mice (B6;129S-$Sparc^{tm1we}$/J) were purchased from Charles River (Margate, UK) [26]. *LSL-*$Kras^{G12D}$;*p48-Cre* (KC) mice (129Sv and C57BL/6) were obtained from the Tuveson group [22]. KC mice develop acinar to ductal metaplasia (ADMs) and PanINs at an early age and slowly progress to advanced and metastatic PDAC after a long latency (usually >12 months) [22]. The model recapitulates the full spectrum of histopathological and clinical features of human PDAC. $Kras^{G12D}$ and *p48-Cre* mice were both crossed with $SPARC^{-/-}$ mice, and subsequent crossing of $Kras^{G12D}$;$SPARC^{+/-}$ mice with *p48-Cre*;$SPARC^{+/-}$ mice resulted in KC-$SPARC^{WT}$ and KC-$SPARC^{-/-}$ mice with a mixed background (129SvJ and C57BL/6). All animal experiments were carried out using protocols approved by the Institutional Animal Care and Use Committee at the University Medical Centre Göttingen. Mice were housed at a 12 h light, 12 h dark rhythm.

2.2. Therapeutic intervention and survival studies

KC-$SPARC^{WT}$ and KC-$SPARC^{-/-}$ mice were subjected to treatment after detection of pancreatic tumours of at least 0.5 cm as described before [27]. For pharmacokinetic studies, 12–15 months old KC-$SPARC^{WT}$ and KC-$SPARC^{-/-}$ mice were treated with gemcitabine (100 mg/kg body weight) once. Gemcitabine hydrochloride (Sigma, USA) was resuspended in sterile normal saline at 10 mg/ml. All tissues were harvested 2 h after the last gemcitabine dose for further analysis as previously described [25]. The 2 h time point was

previously found to be the Tmax for intratumoural dFdCTP in KPC pancreatic tumours [23,25]. For survival analysis, endpoint criteria for KC-*SPARC*^{WT} and KC-*SPARC*$^{-/-}$ were defined as 20% body weight loss, general morbidity, lethargy, lack of social interaction or development of ascites.

2.3. Liquid chromatography-mass spectrometry/mass spectrometry (LC-MS/MS)

Fresh frozen tumour samples were homogenised and extracted in 50% acetonitrile with 25 µg/ml tetrahydrouridine (THU, Calbiochem). Samples were then prepared and analysed in one batch as previously described [23,24]. Briefly, a standard curve was generated using standards of known concentration of each analyte spiked into blank tumour homogenate, and quality control samples (at lower limit of quantification, low, medium and high concentration) were included at the beginning and end of the run to confirm batch acceptance. LC-MS/MS for gemcitabine (dFdC), dFdU and dFdCTP was performed using PGC Hypercarb columns (Thermo Fisher Scientific, UK) and a Thermo Scientific TSQ Vantage triple stage quadrupole mass spectrometer with Vanquish Quaternary UPLC, data acquired with LC Quan 2.5.6.

2.4. Cell lines

Murine CAFs and cancer cells were isolated from freshly isolated pancreata derived from KC-*SPARC*^{WT} and KC-*SPARC*$^{-/-}$ mice as previously described and maintained in DMEM (Invitrogen, USA) +10% FBS and 1% non-essential amino acids. (Thermo Fisher, USA). [11]. The following human pancreatic cancer cell lines were used: L3.6pl, Panc-1, Capan-1, Bxpc-3. Two immortalised human pancreatic stellate cell lines were used as previously described and abbreviated PSC1 [28], and PSC2 [29].

2.5. Western blot analysis

Western blot analysis was performed as previously described [11]. The following primary antibodies were used: Hsp90 (Cell signaling, USA, #4875, RRID: AB_2233331), SPARC (R&D Systems, USA #AF942, RRID: AB_2286625), mAb SPARC (D10F10, Cell Signaling; RRID: AB_10860770), and collagen I (Abcam, ab21286, RRID: AB_446161). Membranes were incubated with secondary HRP-antibodies (Jackson ImmunoResearch, USA) and developed using chemiluminescence substrate Plus-ECL (PerkinElmer Inc., USA) and protein bands were detected at the ChemiDoc^{TM} XRS+ imaging system (Bio-Rad Laboratories GmbH, Germany) using Image Lab Software (version 5.2.1, RRID: SCR 014210).

2.6. Histological examination and laser fluorescence microscopy

Tissues were fixed in 10% neutral buffered formalin (Sigma) for 24 h and transferred to 70% ethanol. Tissues were embedded in paraffin, and 3–5 µm sections were processed for H&E staining, immunohistochemistry and co-immunofluorescence using standard protocols as previously described [30]. The following antibodies and kits were used: SPARC (R&D Systems, AF942, 1:100, RRID: AB_2286625), α-SMA (Dako, Clone 1A4, 1:250, RRID: AB_2335694), CC3 (Cell signaling, 9664L, 1:100, RRID: AB_2070042) and Ki67 (Thermo Scientific, RM-9106, 1:200, RRID: AB_2341197), CD31 (BD Biosciences, 553370, 1:100, RRID: AB_394816). Pictures were taken with 40× magnification with an Olympus DP27 camera and the Olympus cellSens Entry 1.12 software.

2.7. Extracellular matrix stains

The following reagents were used for special extracellular matrix stains: Picrosirius Red Stain Kit (Polysciences Inc., Cat. 24901-250), Masson trichrome staining kit (Polysiences Inc., Cat. 25088-1), Weigert's iron hematoxylin kit (Sigma) and hyaluronic acid binding protein (Calbiochem, Cat. 385911). The stainings were performed according to standard protocols on formalin fixed, paraffin embedded mouse tissues. Images were acquired as described above.

2.8. Methods of quantification

2.8.1. Automated quantification

Automated quantification of picrosirius, hyaluronic acid and α-SMA staining area was conducted by using Fiji/ImageJ (Fiji, RRID: SCR 002285) applying a low threshold to account for background staining of necrotic tumour areas. For Masson trichrome, CD31 and herovici stainings, automated quantification was performed using the Ariol SL-50 and Aperio XT automated scanning system and Imagescope 10 software (Leica Biosystems, Germany) as described previously [31].

2.8.2. Manual quantification

The following IHC data were manually quantified by counting positive stained cells for CC3 and Ki67 at least 5 HPFs (40× per slide) divided by the number of all nuclei as determined by ImageJ. PanIN and ADM lesions from early (3–4 months old) and late (7–8 months old) KC-*SPARC*^{WT} and KC-*SPARC*$^{-/-}$ mice were semi-quantitatively scored by an expert pancreas pathologist (B.S.) with score 0: normal tissue/no PanIN/no ADM, score 1: <30% ADMs/PanINs of total pancreas tissue area, score 2: 30–70% ADMs/PanINs, score 3: > 70% ADMs/PanINs of total tissue area. For metastasis quantification, 5 serial H&E liver sections were quantified for metastatic burden. Liver metastases ranging from 100 to 200 µm were arbitrarily considered micro-metastases, >200 µm as macro-metastases. Each macro-metastasis was multiplied by 3 for the final metastatic score to account for the different size.

2.9. Statistical analysis

Data are presented as mean ± SD. Statistical analysis was performed using GraphPad Prism 7.03a, (RRID: SCR 002798). $p < .05$ Was considered statistically significant. The individual statistical tests are separately indicated in the figure legends.

3. Results

3.1. SPARC is expressed early during PanIN development, mediates collagen deposition but does not affect PanIN-PDAC progression

To investigate the effects on ECM formation, PanIN progression and drug delivery upon oncogenic Kras^{G12D} activation, we crossed SPARC$^{-/-}$ mice (B6;129S-Sparc^{tm1Hwe}/J) with KC mice to obtain KC-*SPARC*$^{-/-}$ and KC-*SPARC*^{WT} control mice. Germline SPARC ablation did not impair normal pancreas development and weight (Fig. 1A, B). In analogy to humans, immunohistochemistry revealed no expression in healthy pancreas tissue, whereas SPARC was expressed in activated fibroblasts around PanINs and in the tumour stroma of invasive murine PDAC (Fig. 1C).

Subsequently, we separated both KC-*SPARC*$^{-/-}$ and KC-*SPARC*^{WT} mice into two cohorts to assess the role of SPARC during different stages of PanIN progression: early ADM and PanIN progression (3–4 months old, $n \geq 7$ mice per cohort), and advanced PanIN lesions (7–8 months old, $n \geq 8$ mice per cohort) (Fig. 1D). Notably, SPARC ablation resulted in a dramatic reduction in overall and mature collagen (Fig. 1E, F; $p < .001$).

In line with immunohistochemistry, isolation of fibroblasts and epithelial cells from advanced PanIN lesions from both genotypes

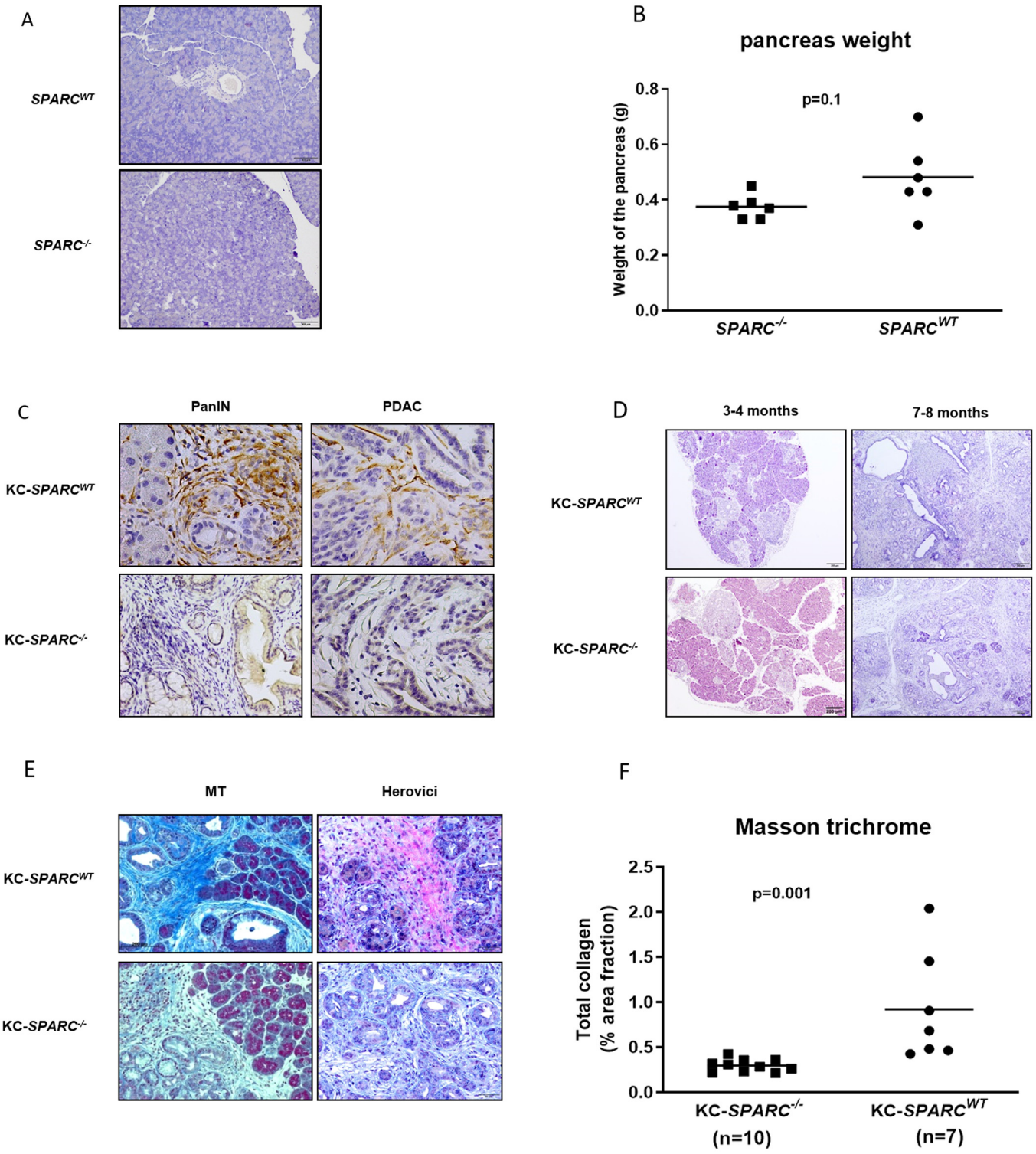

Fig. 1. A: Representative H&E stainings of 10 months old *SPARC*$^{-/-}$ mice and control wildtype mice show normal histological architecture of the pancreas. B: Pancreas weight of *SPARC*$^{-/-}$ mice ($n = 6$) and control wildtype mice ($n = 6$)($p = .1$, Mann-Whitney-*U* test). C: SPARC immunohistochemistry in KC-*SPARC*^{WT} mice shows robust expression in fibroblasts around PanINs (left upper panel) and cancer associated fibroblasts (right upper panel). Lower panel reveals no immunoreactivity for SPARC in KC-*SPARC*$^{-/-}$ mice. D: H&E stainings of KC-*SPARC*^{WT} and KC-*SPARC*$^{-/-}$ mice from early and late PanINs. E: Masson trichrome (MT) and Herovici staining in pancreata from KC-*SPARC*^{WT} and KC-*SPARC*$^{-/-}$ reveals depletion of collagen matrix (blue), and reduction of mature collagen fibres (red) in KC-SPARC$^{-/-}$ mice (7–8 months). F: Automated quantification of MT staining in KC-*SPARC*^{WT} ($n = 7$) and KC-*SPARC*$^{-/-}$ ($n = 10$) ($p < .001$, Mann-Whitney-U test). (For interpretation of the references to colour in this figure legend, the reader is referred to the web version of this article.)

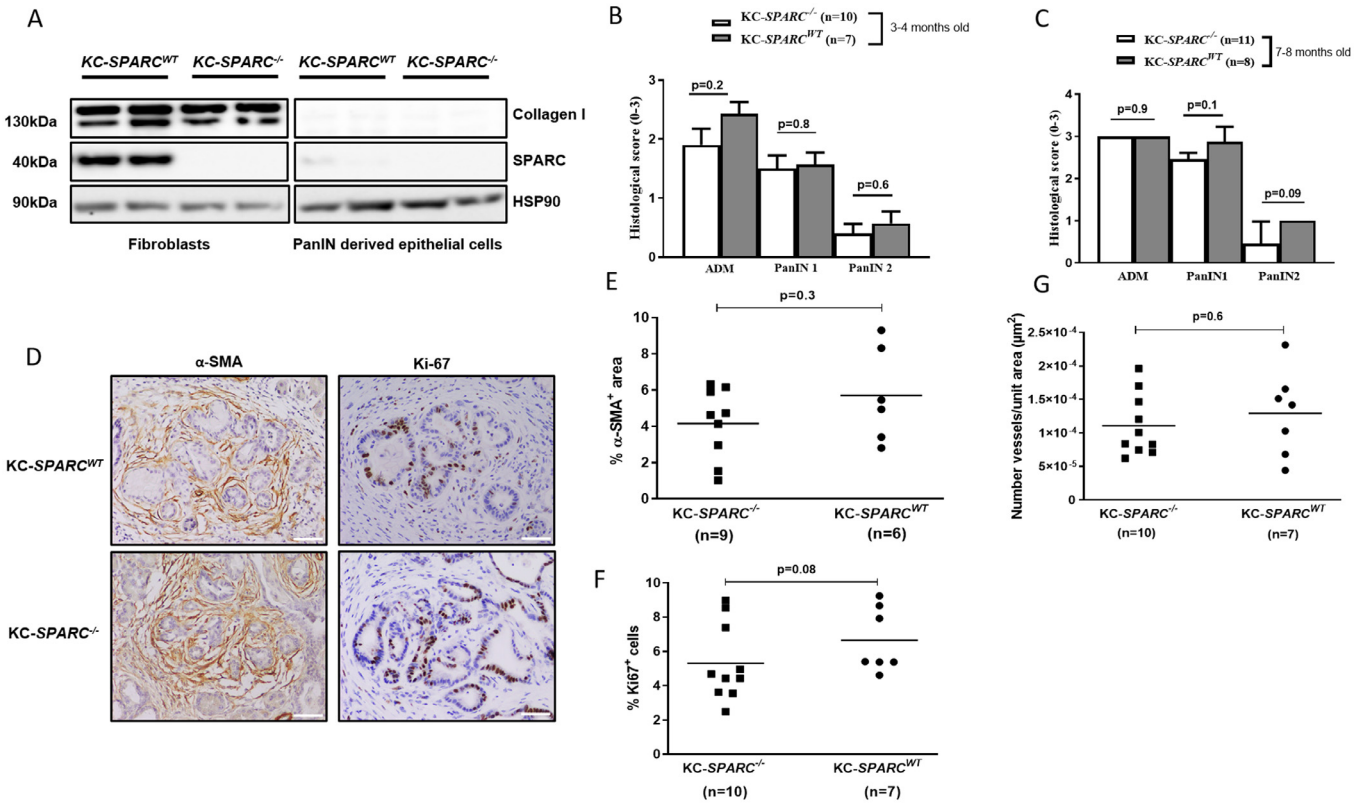

Fig. 2. A: Western blot analysis showing robust SPARC expression in isolated fibroblasts from KC-*SPARC*^{WT} with simultaneous collagen-I expression, whereas fibroblasts from KC-*SPARC*$^{-/-}$ and epithelial tumour cells are devoid of SPARC expression ($n=2$ for each cell line). KC-*SPARC*$^{-/-}$ fibroblasts express collagen as SPARC is not involved in collagen synthesis but assembly and deposition. B, C: Semiquantitative analysis (score 0–3) of early (3–4 months old) and late (7–8 months old) ADM and PanIN I-II lesions in KC-*SPARC*^{WT} ($n=7/8$) and KC-*SPARC*$^{-/-}$ ($n=10/11$) mice. D: Immunohistochemistry for α-SMA and Ki67 in PanIN+ADM pancreatic tissue from KC-*SPARC*^{WT} and KC-*SPARC*$^{-/-}$mice (3–4 months old). E: Automated quantification of α-SMA immunohistochemistry in preneoplastic tissues from KC-*SPARC*^{WT} and KC-*SPARC*$^{-/-}$ mice (3–4 months old). F: Manual quantification of Ki67 immunohistochemistry showing no significant differences between KC-*SPARC*^{WT} and KC-*SPARC*$^{-/-}$mice (3–4 months old). G: Automated quantification of CD31 immunohistochemistry in preneoplastic tissues from KC-*SPARC*^{WT} ($n=7$) and KC-*SPARC*$^{-/-}$ ($n=10$) mice (3–4 months old, p-values all calculated by Mann-Whitney-U test).

($n=2$ for each genotype) showed no expression of SPARC in epithelial cells, and strong expression in fibroblasts derived from KC-*SPARC*^{WT} (Fig. 2A). Comparable results were obtained from a set of human PDAC cell lines and PSCs by Western blot analysis (Suppl Fig. 1A).

In line with immunohistochemistry, isolation of fibroblasts and epithelial cells from advanced PanIN lesions from both genotypes ($n=2$ for each genotype) showed no expression of SPARC in epithelial cells, and strong expression in fibroblasts derived from KC-*SPARC*^{WT} (Fig. 2A). Comparable results were obtained from a set of human PDAC cell lines and PSCs by Western blot analysis (Suppl Fig. 1A).

Notably, as SPARC regulates collagen deposition in vivo, but not collagen secretion, collagen levels were comparable between the two genotypes in cultured fibroblasts (Fig. 2A).

Semi-quantitative pathological scoring (0–3) revealed no significant differences in ADM and PanIN progression upon SPARC depletion at both time points (Fig. 2B, C).

Additional immuno-histochemical analysis showed no significant changes in α-SMA positive fibroblasts or overall proliferation rate (Fig. 2D–F). Moreover, mean vessel density (CD31) was unchanged in PanINs and ADMs upon SPARC ablation (Fig. 2G). This is in contrast to previous data where lack of SPARC enhanced vascular function in an orthotopic mouse model of PDAC [19].

3.2. SPARC ablation significantly reduces survival in the KC mouse model and reveals increased frequency of tumour related symptoms

In order to investigate the effects of peritumoural SPARC as marker for the "activated" tumour stroma, we aged KC-*SPARC*$^{-/-}$ ($n=53$) and KC-*SPARC*^{WT} control mice ($n=29$) for >12 months. Tumour development mostly occurred after 12 months (range 5–21 months). Tumour frequency in both cohorts was not significantly different for KC-SPARC$^{-/-}$ and KC-SPARC^{WT} mice (49% vs. 65%, Fig. 3A). Tumour related survival was defined according to established endpoint criteria such as ascites, inactivity, jaundice, and significant weight loss. In a separate survival cohort, tumour bearing KC-*SPARC*$^{-/-}$ ($n=25$) showed a significantly shortened survival from birth compared to tumour bearing KC-*SPARC*^{WT} mice ($n=16$; 280d vs 485d, $p<.03$, Log-rank test, Fig. 3B). Tumour tissue was analysed regarding ECM formation and showed a dramatic reduction in collagen content and organization (Fig. 3C–E).

However, SPARC nullizygosity neither affected the proportion of α-SMA positive fibroblasts nor intratumoural hyaluronic acid accumulation (Fig. 3F, Suppl Fig. 1B, C). Furthermore, tumour proliferation and apoptosis rate were not significantly changed between the two cohorts of mice (Suppl Fig. 1D, E). All tumours were graded from G1-G4 with the majority of tumours being G2 for KC-SPARC$^{-/-}$ (13/23; 57%) and KC-SPARC^{WT} (10/18; 56%) and no apparent association of SPARC expression and differentiation.

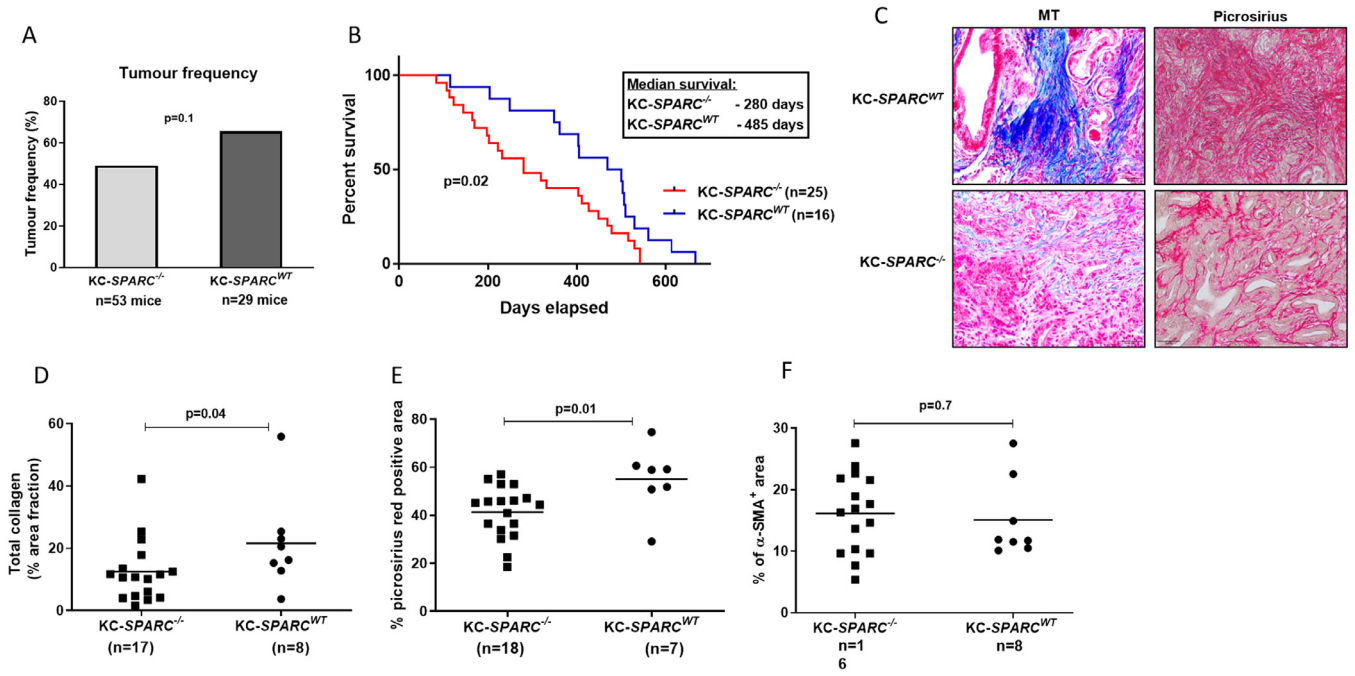

Fig. 3. A: PDAC frequency in KC-*SPARC*^{WT} ($n=29$, 65% tumour frequency) and KC-*SPARC*$^{-/-}$ ($n=53$; 49% tumour frequency, $p=.1$, Fishers Exact test). B: Survival analysis of tumour bearing KC-*SPARC*^{WT} ($n=16$) and KC-*SPARC*$^{-/-}$ ($n=25$) mice shows significantly reduced survival of KC-SPARC$^{-/-}$ mice (280 days versus 485 days, $p=.02$, log-rank-test). C: Masson trichrome (MT) and picrosirius red staining in pancreatic tumours derived from KC-*SPARC*^{WT} and KC-*SPARC*$^{-/-}$ mice shows reduced overall collagen, in particular collagen I and III (picrosirius red). D: Automated quantification of MT in tumours from KC-*SPARC*^{WT} ($n=8$) and KC-*SPARC*$^{-/-}$ ($n=17$) mice ($p<.05$, Mann Whitney *U* test) E: Automated quantification of picrosirius red in tumours from KC-*SPARC*^{WT} ($n=7$) and KC-*SPARC*$^{-/-}$ ($n=18$) mice. Collagen is significantly reduced in KC-SPARC$^{-/-}$ mice ($p=.01$; Mann Whitney U test). F: Automated quantification of α-SMA immunohistochemistry in tumours from KC-*SPARC*^{WT} ($n=8$) and KC-*SPARC*$^{-/-}$ ($n=16$) mice ($p=.7$, Mann-Whitney-U test). (For interpretation of the references to colour in this figure legend, the reader is referred to the web version of this article.)

However, SPARC nullizygosity neither affected the proportion of α-SMA positive fibroblasts nor intratumoural hyaluronic acid accumulation (Fig. 3F, Suppl Fig. 1B, C). Furthermore, tumour proliferation and apoptosis rate were not significantly changed between the two cohorts of mice (Suppl Fig. 1D, E). All tumours were graded from G1-G4 with the majority of tumours being G2 for KC-SPARC$^{-/-}$ (13/23; 57%) and KC-SPARC^{WT} (10/18; 56%) and no apparent association of SPARC expression and differentiation.

3.3. Clinical symptoms are more severe in KC-SPARC$^{-/-}$ mice, but frequency of liver metastasis is not affected by SPARC ablation

Since macrophage derived SPARC was shown to be involved in metastasis formation using an orthotopic model [32], we quantified micro- and macro-metastases to the liver, however, no significant difference was observed upon SPARC depletion (Fig. 4A, B). Notably, clinical symptoms such as ascites, jaundice and diarrhoea occurred more frequently in KC-*SPARC*$^{-/-}$ (Table 1), providing a possible explanation for the shortened survival despite the comparable tumour kinetics.

Table 1
Clinical symptoms in KC-*SPARC*^{WT} ($n=18$) and KC-*SPARC*$^{-/-}$ ($n=26$) mice showing a more severe phenotype in KC-*SPARC*$^{-/-}$ mice.

Clinical signs	KC-*SPARC*$^{-/-}$ ($n=26$)	KC-*SPARC*^{WT} ($n=18$)
Ascites	4 (15%)	0
Jaundice	4 (15%)	1
Diarrhoea	2 (8%)	0

p-values for ascites ($p=.1$), jaundice ($p=.6$), and diarrhoea ($p=.5$) using Fishers Exact test.

3.4. SPARC ablation and subsequent collagen reduction in murine PDAC does not impair gemcitabine delivery or immediate efficacy

Since SPARC was suggested as negative predictive factor for the treatment with gemcitabine [16], we investigated whether SPARC dependent collagen deposition would impinge on gemcitabine metabolism and effectiveness. To this end, we treated tumour-bearing 12–15 months old KC-*SPARC*$^{-/-}$ ($n=10$) and KC-*SPARC*^{WT} mice ($n=6$) with a single dose of 100 mg/kg gemcitabine. Pancreatic tumour samples were taken 2 h after gemcitabine administration as previous data had shown that peak gemcitabine levels and gemcitabine induced cell death were reached after 2 h [25].

Tumour samples were subjected to LC-MS/MS analysis and showed no significant differences for the gemcitabine prodrug 2′,2′-difluorodeoxycytidine (dFdC) as well as for the activated and cytotoxic form of gemcitabine 2′,2′-difluorodeoxycytidine-5′-triphosphate (dFdCTP) despite the differences in collagen content (Fig. 4C, D). Furthermore, the immediate therapeutic response did not differ between KC-*SPARC*$^{-/-}$ and KC-*SPARC*^{WT} tumours as evidenced by a comparable number of cleaved-caspase 3 positive tumour cells (Fig. 4E).

4. Discussion

PDAC is characterised by the accumulation of large amounts of ECM components such as collagen and hyaluronic acid, as well as abundant fibro-inflammatory cells that surround neoplastic cells at large numbers. Over the last years, accumulating evidence suggests that the tumour stroma can both restrain and promote disease progression and therapeutic resistance [7,33,34]. However, due to the complex composition of cellular and acellular components of the stroma, it is often not clear which components accelerate and attenuate tumour progression. Furthermore, a highly debated and

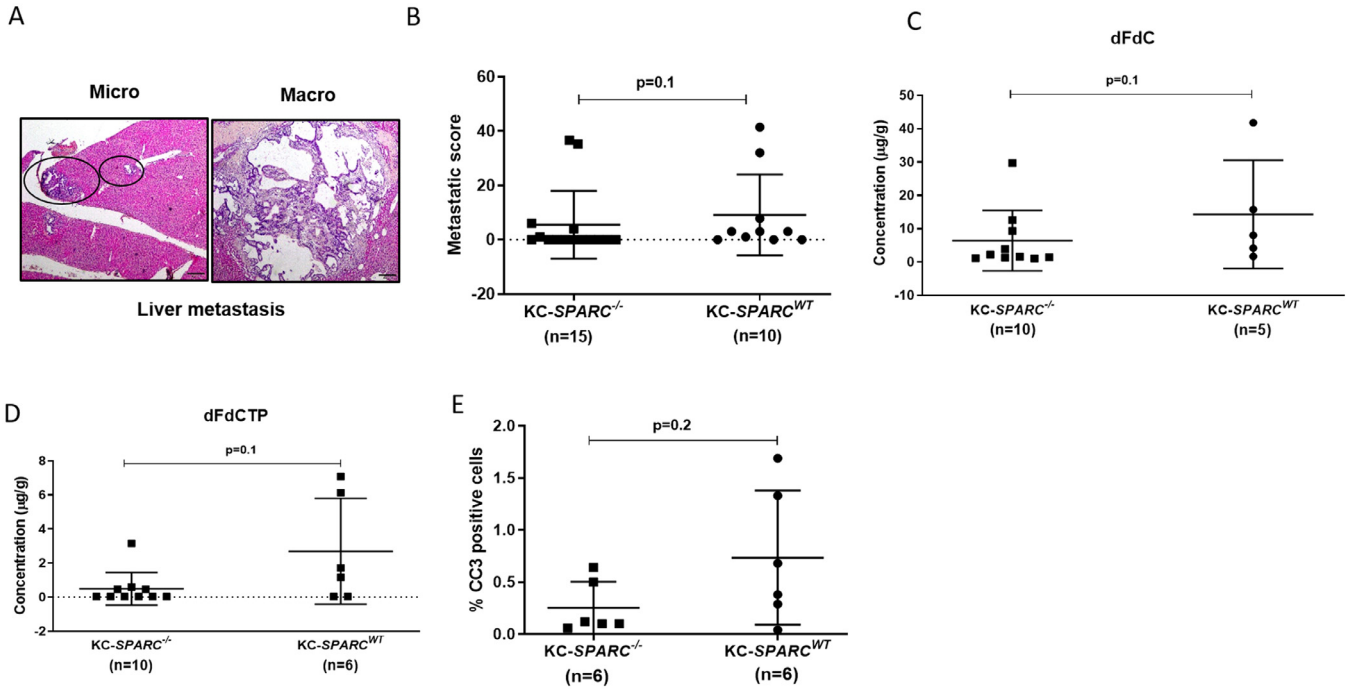

Fig. 4. A: H&E staining from micro-metastases (circles left picture) and macro-metastases of the liver in KC-SPARC^{WT} mice. B: Manual quantification of macro- and micro-metastases in KC-SPARC^{WT} ($n = 10$) and KC-SPARC$^{-/-}$ ($n = 15$). C + D Tumour tissues from KC-*SPARC*^{WT} ($n \geq 5$) and KC-*SPARC*$^{-/-}$ mice ($n = 10$) were assessed for gemcitabine metabolites 2 h after injection of 100 mg/kg gemcitabine by LC-MS/MS. Native gemcitabine (dFdC) and the active form of gemcitabine 2′,2′-difluorodeoxyuridine-5′-triphosphate (dFdCTP) were not significantly altered between the two genotypes. E: Manual quantification of CC3 immunohistochemistry in tumours from KC-*SPARC*^{WT} ($n = 6$) and KC-*SPARC*$^{-/-}$ ($n = 6$) mice upon 1 dose of gemcitabine at 100 mg/kg. Mann-Whitney-U test was used for calculation of *p*-values.

largely unsolved question is whether this desmoplastic reaction in PDAC creates biophysical barriers for drug delivery that may, at least partly, explain the highly chemoresistant phenotype of human PDAC. Consequently, despite several promising preclinical approaches to therapeutically target the tumour stroma [5–8,10,25], none of the anti-stromal compounds have so far succeeded in clinical trials [4]. Stromal and epithelial subtyping conducted by RNA sequencing and often combined with laser capture microdissection has recently revealed “activated” and “normal” stromal subtypes in PDAC patients that are strongly correlated with prognosis [13,35]. The fact that SPARC is one of the most prominently expressed transcripts in the “activated” stroma subtype that is correlated with worse survival [13], and the fact that SPARC was suggested as potential biomarker for gemcitabine response [16], led us to investigate the expression, function and preclinical relevance of peritumoural SPARC in a genetically engineered mouse model of PDAC.

Therefore, we depleted the matricellular protein SPARC that is centrally involved in collagen maturation and deposition in the KC mouse model to investigate the effect of SPARC on the PanIN-PDAC progression. Notably, our results show that SPARC ablation caused a significant reduction in overall and mature collagen deposition during preneoplastic and invasive tumour stages. Despite the fact that tumour bearing KC-*SPARC*$^{-/-}$ mice lived significantly shorter compared to their tumour bearing wildtype littermates, hallmark features such as PanIN progression, epithelial cell proliferation, CAF viability, and invasiveness, angiogenesis or metastatic frequency were not altered by SPARC expression. Thus, the shortened survival may likely be caused by an increase in tumour related symptoms such as ascites, diarrhoea and jaundice, but not by more aggressive and metastatic tumours per se. This more severe phenotype might be caused by systemic effects of global SPARC depletion in mice upon tumour induction, but not specifically by alterations of stromal SPARC ablation in pancreatic tumours. Albeit not significantly, it was interesting to note that despite the worse outcome of KC-*SPARC*$^{-/-}$ mice, tumour frequency was lower in KC-*SPARC*$^{-/-}$ compared to KC-*SPARC*^{WT}mice. Conditional genetic deletion of SPARC using a fibroblast-specific promoter such as α-SMA or collagen should be performed and might yield distinctly different results. Previous data generated in orthotopic and genetically engineered mice (*LSL-Kras*^{G12D}; *Cdkn2a*$^{lox/lox}$; *p48*^{Cre}) suggest direct effects of SPARC on angiogenesis and tumour progression that could not be recapitulated in our experiments using the KC-mouse model [17,19], where ADM and PanIN lesions slowly progress, and tumour development occurs only in about 50–60% of mice. These fundamentally different growth kinetics and the more aggressive tumour biology using *LSL-Kras*^{G12D}; *Cdkn2a*$^{lox/lox}$; *p48*^{Cre} mice may have determined the observed phenotype.

Since SPARC was suggested as negative predictive factor for the treatment with gemcitabine [16], we investigated whether SPARC dependent collagen deposition would impinge on gemcitabine metabolism and effectiveness for the first time. In line with previously published data on nab-paclitaxel and SPARC [30,36,37], we did not see significant changes in gemcitabine pharmacokinetics and pharmacodynamics upon genetic SPARC modification.

Therefore, our data suggest that despite the observed collagen reduction, peritumoural SPARC ablation neither determines hallmark features of pancreatic tumour development and progression nor the response to gemcitabine in a genetically engineered model of autochthonous PDAC. However, one potential limitation of our mouse model is that SPARC was deficient in all cells during development thus potentially affecting the results and the phenotype of the mice. Notably, two major cell types of the TME, CAFs and tumour-associated macrophages (TAMs) were recently discovered to actively metabolise and scavenge chemotherapeutic drugs in experimental PDAC [11,38]. Our current findings on SPARC dependent collagen deposition and gemcitabine delivery are in line with these data and point towards a critical role of these cell types for future therapeutic approaches and clinical trial design.

Contributors

A.N., E.H., and V.E. conceived and designed the experiments. A.N., I.R., S.M.B, M.S.·P, R.G.G. performed animal experiments. S.M.B., I.R., M.S.P., and S.K.S. performed cell culture experiments. S.M.B., I.R., M.S.P., S.K.S., P.S., and B.S. performed and analysed histology stainings. FMR and DIJ designed and analysed pharmacokinetic LC-MS/MS experiments. A.N., S.M.B. and E.H. wrote the manuscript. All authors reviewed the manuscript.

Declaration of Competing Interest

The authors declare no conflict of interest.

Acknowledgements

We thank Jutta Blumberg and Ulrike Wegner for expert technical assistance. This work was supported by the Deutsche Krebshilfe (Max Eder group) [110972 and 70113213] to A.N., Deutsche Krebshilfe (Max Eder Group) to S.K.S. [70112999], and (PiPAC Consortium) [70112505] to E.H. and V.E., the Else-Kröner-Fresenius-Stiftung to R.G.G., the MD-fellowship from the Deutsche Gesellschaft für Gastroenterologie, Verdauungs- und Stoffwechselkrankheiten to S.M.B. Cancer Research UK (CRUK) supports the Jodrell Group (D.I.J. and F.M.R.). LC-MS/MS analyses were performed in the PKB core at the CRUK Cambridge Institute. The CRUK Cambridge Institute (Li Ka Shing Centre) was generously funded by CK Hutchison Holdings Limited, the University of Cambridge, The Atlantic Philanthropies and a range of other donors.

Appendix A. Supplementary data

Supplementary data to this article can be found online at https://doi.org/10.1016/j.ebiom.2019.09.024.

References

[1] Neesse A, et al. Stromal biology and therapy in pancreatic cancer. Gut 2011;60(6):861–8.
[2] Vennin C, et al. Reshaping the tumor Stroma for treatment of pancreatic cancer. Gastroenterology 2018;154(4):820–38.
[3] Mahajan UM, et al. Immune cell and stromal signature associated with progression-free survival of patients with resected pancreatic ductal adenocarcinoma. Gastroenterology 2018;155(5):1625–39 e2.
[4] Neesse A, et al. Stromal biology and therapy in pancreatic cancer: ready for clinical translation? Gut 2019;68(1):159–71.
[5] Jacobetz MA, et al. Hyaluronan impairs vascular function and drug delivery in a mouse model of pancreatic cancer. Gut 2013;62(1):112–20.
[6] Nagathihalli NS, et al. Signal transducer and activator of transcription 3, mediated remodeling of the tumor microenvironment results in enhanced tumor drug delivery in a mouse model of pancreatic cancer. Gastroenterology 2015;149(7):1932–43 e9.
[7] Olive KP, et al. Inhibition of hedgehog signaling enhances delivery of chemotherapy in a mouse model of pancreatic cancer. Science 2009;324(5933):1457–61.
[8] Provenzano PP, et al. Enzymatic targeting of the stroma ablates physical barriers to treatment of pancreatic ductal adenocarcinoma. Cancer Cell 2012;21(3):418–29.
[9] Vennin C, et al. Transient tissue priming via ROCK inhibition uncouples pancreatic cancer progression, sensitivity to chemotherapy, and metastasis. Sci Transl Med 2017;9:384.
[10] Chauhan VP, et al. Angiotensin inhibition enhances drug delivery and potentiates chemotherapy by decompressing tumour blood vessels. Nat Commun 2013;4:2516.
[11] Hessmann E, et al. Fibroblast drug scavenging increases intratumoural gemcitabine accumulation in murine pancreas cancer. Gut 2018;67(3):497–507.
[12] Kim EJ, et al. Pilot clinical trial of hedgehog pathway inhibitor GDC-0449 (vismodegib) in combination with gemcitabine in patients with metastatic pancreatic adenocarcinoma. Clin Cancer Res 2014;20(23):5937–45.
[13] Moffitt RA, et al. Virtual microdissection identifies distinct tumor- and stroma-specific subtypes of pancreatic ductal adenocarcinoma. Nat Genet 2015;47(10):1168–78.
[14] Sato N, et al. SPARC/osteonectin is a frequent target for aberrant methylation in pancreatic adenocarcinoma and a mediator of tumor-stromal interactions. Oncogene 2003;22(32):5021–30.
[15] Infante JR, et al. Peritumoral fibroblast SPARC expression and patient outcome with resectable pancreatic adenocarcinoma. J Clin Oncol 2007;25(3):319–25.
[16] Sinn M, et al. SPARC expression in resected pancreatic cancer patients treated with gemcitabine: results from the CONKO-001 study. Ann Oncol 2014;25(5):1025–32.
[17] Aguilera KY, et al. Collagen signaling enhances tumor progression after anti-VEGF therapy in a murine model of pancreatic ductal adenocarcinoma. Cancer Res 2014;74(4):1032–44.
[18] Arnold S, et al. Forced expression of MMP9 rescues the loss of angiogenesis and abrogates metastasis of pancreatic tumors triggered by the absence of host SPARC. Exp Biol Med (Maywood) 2008;233(7):860–73.
[19] Arnold SA, et al. Lack of host SPARC enhances vascular function and tumor spread in an orthotopic murine model of pancreatic carcinoma. Dis Model Mech 2010;3(1–2):57–72.
[20] Heeg S, et al. ETS-transcription factor ETV1 regulates stromal expansion and metastasis in pancreatic cancer. Gastroenterology 2016;151(3):540–53 e14.
[21] Puolakkainen PA, et al. Enhanced growth of pancreatic tumors in SPARC-null mice is associated with decreased deposition of extracellular matrix and reduced tumor cell apoptosis. Mol Cancer Res 2004;2(4):215–24.
[22] Hingorani SR, et al. Preinvasive and invasive ductal pancreatic cancer and its early detection in the mouse. Cancer Cell 2003;4(6):437–50.
[23] Bapiro TE, et al. Gemcitabine diphosphate choline is a major metabolite linked to the Kennedy pathway in pancreatic cancer models in vivo. Br J Cancer 2014;111(2):318–25.
[24] Bapiro TE, et al. A novel method for quantification of gemcitabine and its metabolites 2′,2′-difluorodeoxyuridine and gemcitabine triphosphate in tumour tissue by LC-MS/MS: comparison with (19)F NMR spectroscopy. Cancer Chemother Pharmacol 2011;68(5):1243–53.
[25] Neesse A, et al. CTGF antagonism with mAb FG-3019 enhances chemotherapy response without increasing drug delivery in murine ductal pancreas cancer. Proc Natl Acad Sci U S A 2013;110(30):12325–30.
[26] Gilmour DT, et al. Mice deficient for the secreted glycoprotein SPARC/osteonectin/BM40 develop normally but show severe age-onset cataract formation and disruption of the lens. EMBO J 1998;17(7):1860–70.
[27] Goetze RG, et al. Utilizing high resolution ultrasound to monitor tumor onset and growth in genetically engineered pancreatic cancer models. J Vis Exp 2018(134).
[28] Hwang RF, et al. Cancer-associated stromal fibroblasts promote pancreatic tumor progression. Cancer Res 2008;68(3):918–26.
[29] Jesnowski R, et al. Immortalization of pancreatic stellate cells as an in vitro model of pancreatic fibrosis: deactivation is induced by matrigel and N-acetylcysteine. Lab Invest 2005;85(10):1276–91.
[30] Neesse A, et al. SPARC independent drug delivery and antitumour effects of nab-paclitaxel in genetically engineered mice. Gut 2014;63(6):974–83.
[31] Frese KK, et al. nab-Paclitaxel potentiates gemcitabine activity by reducing cytidine deaminase levels in a mouse model of pancreatic cancer. Cancer Discov 2012;2(3):260–9.
[32] Sangaletti S, et al. Macrophage-derived SPARC bridges tumor cell-extracellular matrix interactions toward metastasis. Cancer Res 2008;68(21):9050–9.
[33] Ozdemir BC, et al. Depletion of carcinoma-associated fibroblasts and fibrosis induces immunosuppression and accelerates pancreas cancer with reduced survival. Cancer Cell 2014;25(6):719–34.
[34] Rhim AD, et al. Stromal elements act to restrain, rather than support, pancreatic ductal adenocarcinoma. Cancer Cell 2014;25(6):735–47.
[35] Maurer C, et al. Experimental microdissection enables functional harmonisation of pancreatic cancer subtypes. Gut 2019;68(6):1034–43.
[36] Kim H, et al. SPARC-independent delivery of nab-paclitaxel without depleting tumor stroma in patient-derived pancreatic cancer Xenografts. Mol Cancer Ther 2016;15(4):680–8.
[37] Hidalgo M, et al. SPARC expression did not predict efficacy of nab-paclitaxel plus gemcitabine or gemcitabine alone for metastatic pancreatic cancer in an exploratory analysis of the phase III MPACT trial. Clin Cancer Res 2015;21(21):4811–18.
[38] Halbrook CJ, et al. Macrophage-released pyrimidines inhibit gemcitabine therapy in pancreatic cancer. Cell Metab 2019;29(6):1390–9 e6.